Electron-impact excitation and collisional transfer into the *nF* levels of helium

J. Ethan Chilton and Chun C. Lin
Department of Physics, University of Wisconsin, Madison, Wisconsin 53706
(Received 29 June 1998)

Through the use of Fourier-transform spectroscopy, the electron-impact optical cross sections for the infrared emissions from the $4F$, $5F$, and $6F$ levels of the helium atom have been measured for gas pressures between 3 and 50 mTorr and incident electron energies from threshold to 200 eV. The very strong pressure dependence of these measured emission cross sections at different energies is in excellent quantitative agreement with the mechanism of excitation transfer from the n^1P levels through collisions with ground-state helium atoms. From our data, we determine the electron-impact cross sections for excitation into the $4F$, $5F$, and $6F$ levels. The effects of the singlet-triplet mixing in the *nF* states on the excitation cross sections are discussed. The excitation data of the $5F$ level are compared with those of $5\,^1S$ and $5\,^1D$. We have also obtained the $n\,^1P \rightarrow nF$ collisional excitation transfer cross sections for $n=4-7$. [S1050-2947(98)03712-3]

PACS number(s): 34.80.Dp, 34.80.My

I. INTRODUCTION

Electron-impact excitation of the helium atom has been a subject of interest for several decades. Measurements of the excitation cross sections for the singlet and triplet *S*, *P*, and *D* levels over a wide range of incident electron energies and final-state quantum numbers have been made using the optical method. These cross sections are used extensively for modeling gaseous discharges and plasmas. However, little work has been reported on the excitation into the *F* levels because radiation from the first few *nF* levels ($n=4-6$) is in the infrared, outside the range of photomultiplier tubes (PMTs) traditionally used in optical measurements for excitation cross sections. The only direct measurement of the fluorescence from *F* levels populated by electron-beam excitation of which we are aware is the experiment of Jobe and St. John using PbS detectors [1]. Their experiments were performed at pressures of 8 mTorr and above and their data display significant pressure effects, making it difficult to extract the excitation cross sections for the *F* levels in the low-pressure limit. Nevertheless, the *F* levels in helium are known to play an important role in the population of other excited levels in different kinds of experiments [2–4]. Even at pressures as low as 3 mTorr, the *F* levels are populated both by direct electron-impact excitation and by transfer from He($n\,^1P$) through collisions with He($1\,^1S$). This mechanism causes the cross section for populating the *F* levels to increase greatly with increasing pressure. Because of the singlet-triplet mixing in the *F* levels [5], the $F \rightarrow D$ decay channel may become the dominant process for populating the ^3D and ^1D levels in electron-impact excitation experiments [6]. Extensive studies of the emission from the *D* levels produced by electron impact at different pressures have been made. Analyses of these data in terms of the *F*-cascade model allow one to infer the cross sections for the *F* levels and to delineate the effects of *F* levels on excitation processes [7–10], even though direct measurements of the cross sections for the *F* levels have remained elusive.

The availability of the weak emission Fourier-transform spectrometer (FTS) has facilitated the study of infrared emissions in electron collision experiments [11,12]. In this paper we report measurements of the optical emissions from the *F* levels excited by electron impact and obtain the associated excitation cross sections. Since the earlier works on the excitation of *F* levels, as well as this one, are closely connected with the collisional transfer process from the $n\,^1P$ levels, a review of this process is given in the next section to facilitate discussion of our results in relation to excitation transfer.

II. SINGLET-TRIPLET MIXING IN THE *nF* LEVELS AND TRANSFER BETWEEN $n\,^1P$ AND *nF*

It has long been known that the excitation functions of the $n\,^3D$ levels exhibit a broad secondary maximum around 100 eV at elevated pressures (above ~30 mTorr) in addition to the narrow (primary) peak at 30 eV characteristic of excitation from a singlet into a triplet level [13]. The secondary peak becomes stronger relative to the primary at increasing pressures. Furthermore, the shape of the secondary peak is similar to that of the excitation functions of the $n\,^1P$ levels. At first these observations were explained by the mechanism suggested by Lees and Skinner for the formation of the secondary peak [14]:

$$\mathrm{He}(1\,^1S) + \mathrm{He}(n\,^1P) \rightarrow \mathrm{He}(1\,^1S) + \mathrm{He}(n\,^3D). \qquad (1)$$

However, this reaction violates Wigner's rule, which requires that total spin be conserved for collisions among atoms conforming to the *LS* coupling. To bridge the transfer from $n\,^1P$ to the triplet levels, Lin and Fowler observed that for the He($1snl$) configurations the exchange integral is much larger than the spin-orbit coupling for $l=0-2$, whereas the reverse is true for $l=3$, because the exchange integral decreases dramatically with increasing l due to the reduced overlap between the $1s$ and nl orbitals [5]. They concluded that the *nF* states of helium, unlike the *S*, *P*, and *D* states, do not conform to the *LS* coupling and should be described instead as a superposition of the $n\,^1F$ and $n\,^3F$ states. The singlet component of the *nF* wave function enables collisional transfer from $n\,^1P$ without violating Wigner's rule and the *nF* atoms so produced may cascade into the

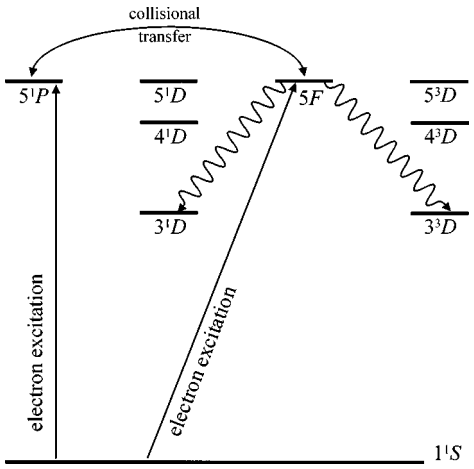

FIG. 1. Partial energy-level diagram for helium. The mixed singlet-triplet $5F$ manifold is populated by direct electron excitation, cascade from higher levels (not shown), and collisional transfer from the $5\,^1P$ level. It is depopulated through radiative transitions to lower levels, as well as by collisional excitation transfer back to the $5\,^1P$ level.

^3D levels through their partial triplet character. The mechanism for the secondary peak in the ^3D is then taken to be

$$\mathrm{He}(1\,^1S)+\mathrm{He}(n\,^1P)\rightarrow\mathrm{He}(1\,^1S)+\mathrm{He}(nF),$$

$$\mathrm{He}(nF)\rightarrow\mathrm{He}(n'\,^3D)+h\nu, \qquad (2)$$

which has been confirmed and used extensively in subsequent works [3,7,8,15]. We illustrate these various excitation mechanisms in Fig. 1.

Much research concerning the singlet-triplet mixing of the F levels and its role in the excitation of the $n\,^3D$ levels has since appeared in the literature. Parish and Mires performed an extensive calculation on the singlet-triplet mixing for several excited states of He and found essentially no mixing for the D states, but significant mixing for the F states [16]. Observation of the $7\,^1D_2\rightarrow 7\,^1F_3$ and $7\,^1D_2\rightarrow 7\,^3F_3$ transitions by Wing and Lamb confirms the presence of the mixed F states [17].

In their experiment with a helium gas discharge, Abrams and Wolga have shown that the Wigner spin rule is obeyed for collisional transfer from the $4\,^3P$ level to the $4\,^1S$, $4\,^1P$, and $4\,^1D$ levels, but does not apply to collisional transfer from $4\,^3F$ [3]. This is in agreement with the prediction of Ref. [5], based on the singlet-triplet mixing of the F states.

Another important feature of the mechanism of Eq. (2) is that the secondary peak in the $n'\,^3D$ excitation is attributed to the cascade from the higher F levels rather than a direct collisional transfer from the $n\,^1P$ atoms as suggested in Eq. (1). Pendleton and Hughes measured the temporal dependence of the fluorescence from the $3\,^3D$ level ($3\,^3D\rightarrow 2\,^3P$) following excitation by a pulsed electron beam [7]. The resulting time-decay curve can be decomposed into two single-exponential components, one with a mean lifetime of 15 ns corresponding to the natural lifetime of the $3\,^3D$ level and the other with a mean lifetime of 130 ± 10 ns. The slow component is attributed to cascade from the F levels since the natural lifetimes for the $4\,^3F$, $5\,^3F$, and $6\,^3F$ levels are 72, 140, and 240 ns, respectively. The slow component was found to increase in its percentage contribution at higher pressure as expected from Eq. (2). Further developments of this time-resolution technique have made it possible to ascertain the portion of the $3\,^3D$ population due to cascade from several individual nF levels [8,9]. This provides an indirect way to determine the $nF\rightarrow 3\,^3D$ emission intensity by measuring the $3\,^3D\rightarrow 2\,^3P$ radiation and its decay curve without actually detecting the $nF\rightarrow 3\,^3D$ radiation. By performing such time-resolution measurements at different pressures it is possible to determine the transfer cross sections between the $n\,^1P$ and nF states and obtain estimates for the nF excitation cross sections.

The mixed nF states generated by transfer from $n\,^1P$ are capable of cascading not only into the lower ^3D levels as shown in Eq. (2) but also into the lower ^1D levels. Thus the nF transfer mechanism predicts a pressure-dependent cascade into the ^1D level and hence the appearance of a broad peak at 100 eV in the ^1D excitation functions at high pressure. This was confirmed experimentally as the 50-eV peak of the $4\,^1D$ excitation function observed at low pressure (2 mTorr) indeed shifts and ultimately transforms into a broad peak at 100 eV at about 130 mTorr [6]. Time-resolution experiments on the $n\,^1D\rightarrow 2\,^1P$ emissions similar to the ones discussed in the preceding paragraph have been reported [8].

The $n\,^1P\rightarrow nF$ transfer and the subsequent cascade to the $3\,^1D$ and $3\,^3D$ levels also have important bearings on measurements of linewidths in plasmas. Momentum transfer associated with collisional excitation of the $3\,^1D$ and $3\,^3D$ levels through this multistep mechanism produces a nonthermal distribution of the Doppler broadening. Such a distortion in the line profile may cause complications in relating the linewidth to gas number density. Distortion of the line profile of emissions from $3\,^1D$ and $3\,^3D$ caused by the excitation transfer mechanism of Eq. (2) has been discussed recently by Su and Nicol [4].

III. METHOD

We use the optical method to measure cross sections for electron-impact excitation of ground-state helium atoms. A more detailed description of the method has been previously published [18]; we present a brief summary here. Consider an electron beam of current I passing through a gas of ground-state atoms of number density n_0, exciting some atoms to level i. The number of photons emitted per beam length per unit time as the atoms decay to some lower level j, Φ_{ij}, is detected and constitutes the primary experimental data that we cast in the form of the *optical emission cross section* for the transition:

$$Q_{ij}^{\mathrm{opt}}\equiv\frac{\Phi_{ij}}{n_0(I/e)}, \qquad (3)$$

where e is the charge of an electron. The sum of all optical emission cross sections from i to lower levels is termed the *apparent excitation cross section* for the level i:

$$Q_i^{\mathrm{app}}=\sum_{j<i}Q_{ij}^{\mathrm{opt}}. \qquad (4)$$

The apparent excitation cross section includes the population of level i by direct excitation as well as indirect mechanisms. In measuring excitation cross sections, the experiments are most often performed at the very-low-pressure regime where secondary processes such as collisional transfer and radiation trapping can be ignored and the measured optical cross sections as defined in Eq. (3) are independent of the pressure. Under this condition one needs to consider only direct excitation and the indirect mechanism of radiative cascade, i.e., populating level i through excitation into a higher level k followed by the $k \rightarrow i$ decay. The cascade component of the total population is simply the sum of the radiation into the level i from all higher levels. Accordingly, the *cascade cross section* is defined as

$$Q_i^{\mathrm{casc}} = \sum_{k>i} Q_{ki}^{\mathrm{opt}}, \tag{5}$$

Thus, in this ideal low-pressure regime, the apparent excitation cross section is the sum of the direct excitation cross section (Q_i^{dir}) and the cascade cross section.

Due to the exceptionally strong collisional transfer involved, the experiments on excitation of the nF levels reported in this paper were mostly not conducted in the ideal low-pressure region and the optical emission and apparent cross sections determined according to Eqs. (3) and (4) are not independent of the pressure. In addition, the $n\,^1P$ levels, which are optically coupled to the ground level, exhibit strong pressure dependence, due to reabsorption of the resonance radiation [1,19]. In these cases, the concept of ''cross section'' may be somewhat questionable in a pedantic sense. Nevertheless, even for measurements made at pressures above the ideal range, we use the term ''optical cross section'' as defined in Eq. (3) to describe the rate of photon emission induced by electron impact and refer to the variations of the optical cross sections and the resulting apparent excitation cross sections with pressure as the ''pressure effect.'' In this section we consider both electron-impact excitation and collisional excitation transfer to determine the pressure dependence of the apparent excitation cross sections. Allowance for the singlet-triplet mixing for the nF levels will be made in the analysis.

At the pressure range of our experiments, the nF levels are populated by direct excitation, cascade, and collisional transfer from $n\,^1P$. Of special interest are the very small energy spacings between the nF and $n\,^1P$ levels (40, 21, and 12 cm^{-1} for $n=4$, 5, and 6, respectively), so that at thermal kinetic energies, atom-atom collisional transfer into the F levels from the ^1P levels of the same n value can occur readily, but transfer between levels of different n is negligible. For a free He atom, the singlet-triplet mixing discussed in Sec. II is limited to LS-basis functions of the same J, i.e., $n\,^1F_3$ mixes with only $n\,^3F_3$, but not with $n\,^3F_2$ and $n\,^3F_4$. Based on this model, transfer from $n\,^1P$ into the two mixed nF_3 states, called nF_3^a and nF_3^b, of wave functions

$$\begin{aligned} \psi(nF_3^a) &= \xi\psi(n\,^1F_3) + \eta\psi(^3F_3) \\ \psi(nF_3^b) &= -\eta\psi(n\,^1F_3) + \xi\psi(^3F_3), \end{aligned} \tag{6}$$

is possible without violating Wigner's rule due to the singlet components in the wave functions. We neglect transfer from $n\,^1P$ to the two purely triplet levels $n\,^3F_2$ and $n\,^3F_4$. As a matter of notation, the two mixed states are collectively referred to as nF_3, whereas the entire nF manifold, including both the mixed and unmixed states, is designated as nF.

Although in our experiment the radiation emitted by the individual members of the nF group is not resolved, the two mixed levels (nF_3) and the two unmixed levels must be analyzed separately. The two mixed levels are populated by direct electron excitation, cascade, and collisional transfer from $n\,^1P$ and are depopulated by radiative decay and collisional transfer into $n\,^1P$. Accordingly, the rate equation for the two mixed levels together (nF_3) is

$$\frac{dn_{nF_3}}{dt} = n_0(I/e)Q_{nF_3}^{\mathrm{dir}} + \sum_{k>nF_3} A_{k\rightarrow nF_3} n_k + c_{n\,^1P\rightarrow nF_3} n_{n\,^1P} - c_{nF_3\rightarrow n\,^1P} n_{nF_3} - \sum_{j<nF_3} A_{nF_3\rightarrow j} n_{nF_3}, \tag{7}$$

where $Q_{nF_3}^{\mathrm{dir}}$ is the sum of the direct excitation cross sections into the two mixed levels, n_{nF_3} refers to the total population of the two nF_3 levels, $n_{n\,^1P}$ is the population density of the $n\,^1P$ level, $c_{a\rightarrow b}$ is the (average) rate of transfer from level(s) a to b through collision with a ground state atom, and $A_{a\rightarrow b}$ is the Einstein A coefficient for the a to b transition. The A coefficients for the $n\,^3F\rightarrow n'\,^3D$ and $n\,^1F\rightarrow n'\,^1D$ transitions are virtually identical and so the total radiative decay rate

$$\sum_{j<nF_3} A_{nF_3\rightarrow j} = A_{nF_3} = A_{nF} \tag{8}$$

is the same for the two mixed levels as well as for the pure LS levels $n\,^3F_2$ and $n\,^3F_4$ and is simply written as A_{nF}. The transfer rate $c_{a\rightarrow b}$ can be expressed in terms of the collisional transfer cross section as

$$c_{a\rightarrow b} = 4n_0\sigma_{a\rightarrow b}(RT/\pi M)^{1/2}, \tag{9}$$

where $\sigma_{a\rightarrow b}$ is the collisional transfer cross section, R the gas constant, T the target gas temperature, and M the atomic mass. The principle of detailed balance requires that the $nF_3\rightarrow n\,^1P$ ''backward'' transfer be related to the $n\,^1P \rightarrow nF_3$ ''forward'' transfer through the statistical weights, i.e.,

$$\sigma_{nF_3\rightarrow n\,^1P} = \frac{3}{14}\,\sigma_{n\,^1P\rightarrow nF_3}. \tag{10}$$

In a steady-state distribution, Eq. (7) becomes

$$n_{nF_3} = \frac{n_0(I/e)Q_{nF_3}^{\mathrm{dir}} + \sum_k A_{k\rightarrow nF_3} n_k + c_{n\,^1P\rightarrow nF_3} n_{n\,^1P}}{c_{nF_3\rightarrow n^1P} + A_{nF_3}}. \tag{11}$$

If we set the transfer rates $c_{i\rightarrow j}$ to zero, the above equation reduces to the case of the ideal low-pressure limit in which the two surviving terms on the right-hand side correspond to

direct excitation and cascade from higher levels k. Since we use the optical method to measure experimentally the number of photons emitted per beam length per time $\Phi_{nF_3\to n'D}$ from specific transitions rather than directly measuring the population densities, we recast Eq. (11) in terms of the measured quantities. Consider the case of $5F_3$. Experimentally, we measure the $5F_3^a\to 3\,^3D$, $5F_3^a\to 3\,^1D$, $5F_3^b\to 3\,^3D$, and $5F_3^b\to 3\,^1D$ emissions that are not resolved and are collectively referred to as $5F_3\to 3D$. The transition probabilities for the $5F_3^a\to 3\,^1D+3\,^3D$ and $5F_3^b\to 3\,^1D+3\,^3D$ groups are virtually the same and are denoted by $A_{5F_3\to 3D}$. To facilitate the analysis of the effects of the gas pressure P we define

$$\beta_{i\to j}=\frac{1}{P}\,c_{i\to j}, \tag{12}$$

which is independent of the helium atom number density. Equation (11) becomes

$$\begin{aligned}\Phi_{5F_3\to 3D}&=A_{5F_3\to 3D}n_{5F_3}\\&=A_{5F_3\to 3D}n_0(I/e)\\&\quad\times\frac{Q^{\rm dir}_{5F_3}+Q^{\rm casc}_{5F_3}+P(n_0J/e)^{-1}\beta_{5\,^1P\to 5F_3}n_{5\,^1P}}{A_{5F_3}+\frac{3}{14}P\beta_{5\,^1P\to 5F_3}}.\end{aligned} \tag{13}$$

In addition to the $5F_3\to 3D$ transitions, our measured radiation intensity includes the emissions from the unmixed levels $5\,^3F_2\to 3\,^3D$ and $5\,^3F_4\to 3\,^3D$, which are not resolved from $5F_3\to 3D$. Since the unmixed levels do not receive transfer from $n\,^1P$, the $5\,^3F_2\to 3\,^3D$ and $5\,^3F_4\to 3\,^3D$ emissions yield the usual optical cross sections $Q^{\rm opt}_{5\,^3F_2\to 3\,^3D}$ and $Q^{\rm opt}_{5\,^3F_4\to 3\,^3D}$, which are not pressure dependent. We express our measured photon emission rate for the entire $5F\to 3D$ group as a pressure-dependent apparent cross section by means of Eq. (3), i.e.,

$$Q^{\rm opt}_{5F\to 3D}(P)=Q^{\rm opt}_{5^3F_2\to 3\,^3D}+Q^{\rm opt}_{5^3F_4\to 3\,^3D}+A_{5F_3\to 3D}\,\frac{(Q^{\rm dir}_{5F_3}+Q^{\rm casc}_{5F_3})+P(n_0J/e)^{-1}(\beta_{5\,^1P\to 5F_3})n_{5\,^1P}}{A_{5F_3}+\frac{3}{14}P\beta_{5\,^1P\to 5F_3}}, \tag{14}$$

and underscore the pressure effect by writing the left-hand side of Eq. (14) as a function of P. The number density $n_{5\,^1P}$ in Eq. (14) is related to the measured optical cross section as

$$n_{5\,^1P}=n_0(I/e)Q^{\rm opt}_{5\,^1P\to 2\,^1S}/A_{5\,^1P\to 2\,^1S}. \tag{15}$$

Because of radiation trapping, the optical cross sections for emission from the $n\,^1P$ levels are known to exhibit pressure dependence even in the absence of collisional transfer (see Sec. V A). To emphasize this point, we use Eq. (15) to rewrite Eq. (14) in terms of the pressure-dependent cross section $Q^{\rm opt}_{5\,^1P\to 2\,^1S}(P)$,

$$Q^{\rm opt}_{5F\to 3D}(P)=Q^{\rm opt}_{5^3F_2\to 3\,^3D}+Q^{\rm opt}_{5^3F_4\to 3\,^3D}+A_{5F_3\to 3D}\,\frac{(Q^{\rm dir}_{5F_3}+Q^{\rm casc}_{5F_3})+P(\beta_{5\,^1P\to 5F_3}/A_{5\,^1P\to 2\,^1S})Q^{\rm opt}_{5\,^1P\to 2\,^1S}(P)}{A_{5F_3}+\frac{3}{14}P\beta_{5\,^1P\to 5F_3}}. \tag{16}$$

The use of experimentally measured cross sections $Q^{\rm opt}_{5\,^1P\to 2\,^1S}(P)$ in Eq. (16) allows for the effects of radiation trapping. In the limit of zero pressure, Eq. (16) reduces to

$$\begin{aligned}Q^{\rm opt}_{5F\to 3\,^3D}(P\to 0)&=Q^{\rm opt}_{5^3F_2\to 3\,^3D}+Q^{\rm opt}_{5^3F_4\to 3\,^3D}\\&\quad+(A_{5F_3\to 3D}/A_{5F})(Q^{\rm dir}_{5F_3}+Q^{\rm casc}_{5F_3})\\&=\Gamma_{5\,^3F\to 3\,^3D}(Q^{\rm app}_{5\,^3F_2}+Q^{\rm app}_{5\,^3F_4}\\&\quad+Q^{\rm app}_{5F_3^a}+Q^{\rm app}_{5F_3^b}),\end{aligned} \tag{17}$$

where Γ is the branching fraction of the transition indicated and we have taken advantage of the fact that the $5F\to nD$ transition probabilities are independent of the spin multiplicity. The pressure dependence of $Q^{\rm opt}_{5F\to 3D}(P)$ in Eq. (16) is due to excitation transfer (the βP terms) as well as the intrinsic pressure dependence of $Q^{\rm opt}_{5\,^1P\to 2\,^1S}(P)$. In our experiment we measure $Q^{\rm opt}_{5F\to 3D}(P)$ and $Q^{\rm opt}_{5\,^1P\to 2\,^1S}(P)$ from 3 to 50 mTorr over the energy range 20–300 eV and use the observed pressure dependence to determine the value of $\beta_{5\,^1P\to 5F_3}$. Once this parameter is known, Eq. (16) can be used to extrapolate our measurements to zero pressure to obtain the sum of the apparent excitation cross sections of the nF levels.

IV. EXPERIMENTAL APPARATUS

To measure the optical cross sections for the $n\,^1P\to 2\,^1S$ and $n^{1,3}D\to 2^{1,3}P$ transitions, which lie in the visible to ultraviolet spectral region, we use a grating monochromator-PMT system. This apparatus has been fully described elsewhere [18,20]. Thus only a brief account is given here. A stainless-steel collision chamber is first evacuated to low pressure and then filled with research grade helium. An electron gun consisting of an indirectly heated BaO cathode and multiple electrostatic focusing and acceleration

grids produces an electron beam, exciting ground-state atoms. Radiation from the collision region passes into a 1.26-m Czerny-Turner spectrometer and is detected by a PMT. The gas pressure is measured with a capacitive manometer and the electron current is captured in a deep Faraday cup. The emission intensity divided by current and pressure yield a value proportional to the optical cross section as defined in Eq. (3). Absolute calibration of the optical measurements is effected by comparing the intensity of the excitation signal with the output of a calibrated standard lamp.

To measure the $nF \rightarrow 3D$ infrared emissions, we use a nearly identical collision chamber and electron gun setup with a FTS in place of the monochromator and PMT. This apparatus was used previously in our investigation of the $2p$ levels of argon [11]. An $In_xGa_{1-x}As$ detector, operating in the (11 750–5900)-cm^{-1} [(0.85–1.7)-μm] spectral region with a resolution of 2 cm^{-1} was used for the $5F$ and $6F$ measurements. The $4F$ levels were detected with the use of an InSb detector covering 7900–3000 cm^{-1} (1.27–3.33 μm). At a given pressure and energy, the FTS recorded and averaged 150 spectral scans. Three such runs were taken at each point and the results averaged. Spectra were corrected for optical transmittance factors and detector sensitivity by observing the output of a calibrated blackbody source as described in Ref. [11]. Using the $In_xGa_{1-x}As$ detector, we extracted the height of the $5F \rightarrow 3D$ peak at 7817 cm^{-1} (1.279 μm), the $6F \rightarrow 3D$ peak at 9161 cm^{-1} (1.092 μm), and the $2\,^3P \rightarrow 2\,^3S$ peak at 9231 cm^{-1} (1.083 μm). Because the $2\,^3P \rightarrow 2\,^3S$ transition is also visible with the monochromator-PMT system, we use that value to normalize our $5F$ and $6F$ cross sections obtained with the $In_xGa_{1-x}As$ detector. In the case of the InSb detector, there is a two-step process to normalize the $4F$ cross sections. An argon discharge tube, which displays several emission lines in the overlap region between the InSb and $In_xGa_{1-x}As$ detectors, is observed with the FTS. We first examine the ratio of the InSb values for the 7287-, 7403-, and 7479-cm^{-1} argon lines to those for the $In_xGa_{1-x}As$ detector. Since the $In_xGa_{1-x}As$ detector has already been normalized to an absolute scale with the helium $2\,^3P \rightarrow 2\,^3S$ line, we can now place the InSb measurement of the $4F$ transition on an absolute scale.

V. RESULTS AND DISCUSSION

A. Optical emission cross section for $n\,^1P \rightarrow 2\,^1S$ and pressure effects

Because of the important role played by the $n\,^1P$ levels in the excitation of the $n\,^1F$ levels, we present in Fig. 2 the optical emission cross sections of the $5\,^1P \rightarrow 2\,^1S$ transitions at 100 eV at various pressures from 0.08 to 50 mTorr. The dramatic increase in cross section with pressure above 2 mTorr is the result of radiation trapping. When the He($5\,^1P$) atoms decay radiatively to the lower $n\,^1S$ and $n\,^1D$ levels, the $5\,^1P \rightarrow 1\,^1S$ resonant photons may be reabsorbed by a nearby ground-state He atom. The He($5\,^1P$) atoms resulting from this reabsorption undergo radiative decay into all lower levels in accordance with the branching fractions. For our experiment this is equivalent to generating additional $5\,^1P \rightarrow 2\,^1S$ emissions at the expense of the resonant radiation. The amount of additional $5\,^1P \rightarrow 2\,^1S$ emission generated by this process depends on the probability of a resonant photon being reabsorbed, which in turn depends on the gas pressure. For a quantitative description, we introduce f as the fraction of the $5\,^1P \rightarrow 1\,^1S$ resonant photons reabsorbed in the collision chamber. Variations of the ''imprisonment factor'' $1-f$ with respect to the gas pressure have been given by Gabriel and Heddle [19]. Using their values of $1-f$, we have calculated the pressure dependence of the $5\,^1P \rightarrow 2\,^1S$ optical emission cross sections due to radiation trapping and found it to be in very good agreement with our measurements as illustrated in Fig. 2. The excitation functions of the $5\,^1P$ levels at six different pressures (3–50 mTorr) are shown in Fig. 3. The shape of the excitation function shows little variation with pressure since at a given pressure the radiation trapping has the same effect on the cross sections regardless of the incident electron energy.

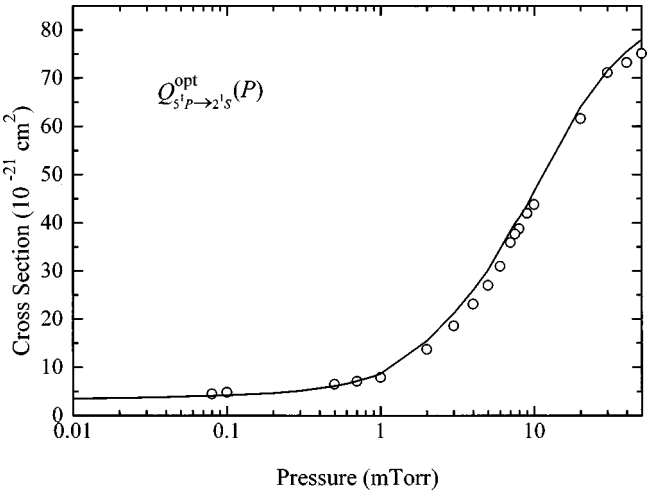

FIG. 2. Optical emission cross section for the $5\,^1P \rightarrow 2^1S$ transition versus pressure at 100-eV incident electron energy. The solid line is the theoretical pressure dependence based on the radiation trapping model of Ref. [19].

Collisional transfer between $5\,^1P$ and $5F$ is another source of the pressure effect of the $5\,^1P \rightarrow 2\,^1S$ optical cross

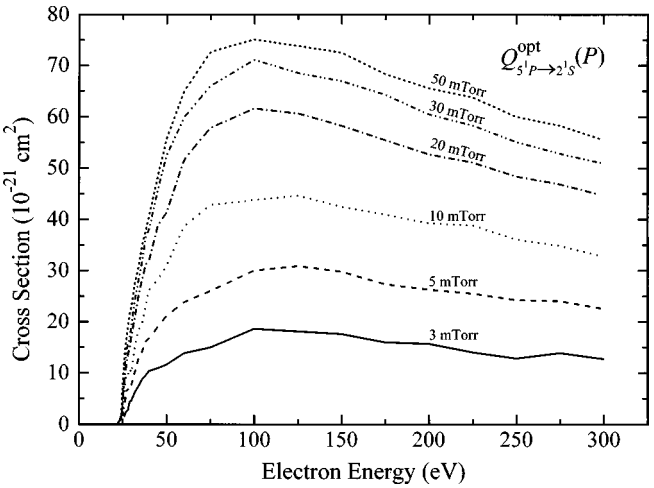

FIG. 3. Excitation functions for the $5\,^1P \rightarrow 2\,^1S$ transition at different pressures. Note the peak near 100-eV incident electron energy. Variation of the magnitude of the cross section is due to resonance radiation reabsorption.

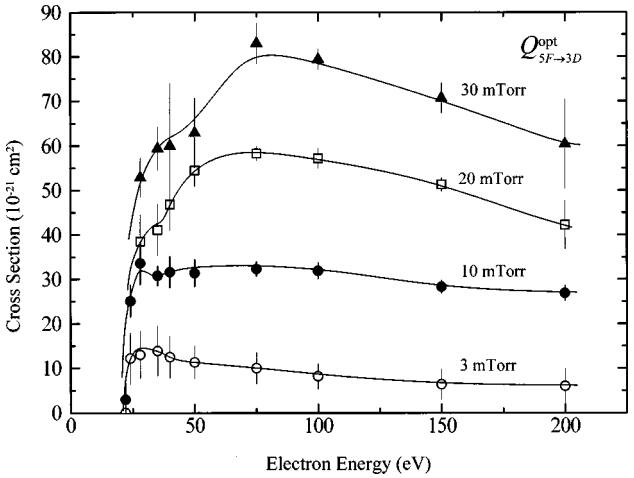

FIG. 4. Optical excitation functions for the $5F\rightarrow 3D$ transition at 3 (○), 10 (●), 20 (□), and 30 mTorr (▲). Smooth curves have been drawn through the data as a guide. As pressure is increased, the shape of the excitation function begins to be influenced by that of the $5\,^1P$ level (Fig. 3).

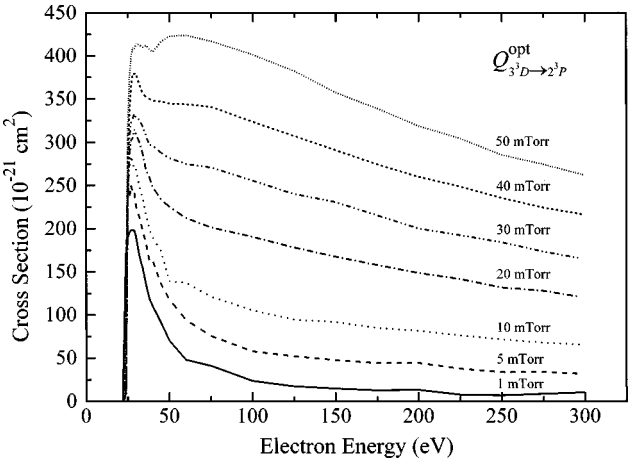

FIG. 5. Excitation functions for the $3\,^3D\rightarrow 2\,^3P$ transition at various pressures. The influence of the $5F$ cascade is clearly seen at high pressures, as a secondary maximum appears near 100 eV.

sections. However, because of the very large $5\,^1P$ cross sections, the $5\,^1P\rightarrow 5F$ transfer causes only a small percentage change in the $5\,^1P\rightarrow 2\,^1S$ emission cross section within the pressure range of Fig. 2. It should be noted, however, that the same transfer produces an enormous change in the $5F\rightarrow 3D$ emission cross section, since the $5F$ levels have much smaller cross sections than do the $5\,^1P$ levels, so the $5\,^1P\rightarrow 5F$ transfer is the dominant contributor to the $5F$ population even at pressures as low as a few mTorr.

B. Analysis of the pressure effects of the $nF\rightarrow 3D$ emission cross sections

Returning to the measurements for the nF levels, we observe the $4F\rightarrow 3D$ transition at incident electron energies between 20 and 300 eV at various pressures up to 50 mTorr. The $5F\rightarrow 3D$ and $6F\rightarrow 3D$ transitions were examined from 3 to 50 mTorr over the same energy range. The $7F\rightarrow 3D$ emission falls outside the $In_xGa_{1-x}As$ spectral region, but could be observed with the monochromator system using an S-1 photocathode. Due to the weak signal and low quantum efficiency of the detector, data were taken between 20 and 50 mTorr and 100 eV only. The emissions from the higher F levels were too weak to be observed. Of all the F level transitions, the one with $n=5$ was the most easily observable. The InSb detector, which is used for the $4F\rightarrow 3D$ transitions, has a lower sensitivity than that of the $In_xGa_{1-x}As$ detector (its detectivity is about a factor of 50 lower), so that the $4F$ line was not observable at very low pressures. Also, the $6F\rightarrow 3D$ line lies close enough to the much larger $2\,^3P\rightarrow 2\,^3S$ transition that its smaller magnitude is often swamped by ripples from incomplete apodization of the $2\,^3P\rightarrow 2\,^3S$ line, making it difficult to extract from the spectrum. Hence most of the following examples will center on the $5F\rightarrow 3D$ transition.

In Fig. 4 we show excitation functions for the $5F\rightarrow 3D$ transition over a range of pressures. It is clear that at a low pressures ($\sim$3 mTorr) the excitation function displays the relatively sharply peaked shape expected of excitation corresponding to dipole-forbidden transitions. However, as pressure is increased, a secondary maximum near 100 eV becomes apparent. By approximately 10 mTorr this secondary peak is of equal magnitude to the low-energy peak and by 20 mTorr this higher-energy peak dominates the excitation function. As discussed later in this section, even at 3 mTorr the $5F$ level receives an appreciable part of its population from $n\,^1P$ transfer. The very slow decline of the 3-mTorr curve in Fig. 4 at high energies represents a distortion of the $5F$ excitation function by this secondary peak. The excitation functions for the $4F\rightarrow 3D$ and $6F\rightarrow 3D$ transitions exhibit similar behaviors. A comparison of Fig. 4 with Fig. 3 suggests that the secondary maxima appearing in the $5F$ excitation functions are related to the 100-eV peak in the $5\,^1P$ excitation function. Because of radiation trapping, the $5\,^1P\rightarrow 2\,^1S$ optical emission cross section increases with pressure. The secondary peak in the optical excitation function of the $5F\rightarrow 3D$ emission as shown in Eq. (16) is to first order proportional to the product of pressure times the $5\,^1P\rightarrow 2\,^1S$ optical cross section. This explains the very dramatic increase of the secondary peak in the $5F$ curves with pressure.

The cascade contribution to the $3\,^3D$ level from the F levels, as discussed in Sec. II, is plainly seen in Fig. 5, which contains excitation functions of the $3\,^3D\rightarrow 2\,^3P$ emission cross sections at seven different pressures from 1 to 50 mTorr. The excitation functions in Figs. 4 and 5 display similar changes in shape with increasing pressure. The $3\,^3D$ level acquires its high-pressure secondary peak from F cascade. The F excitation functions in turn acquire their secondary peak from the $n\,^1P$ level through excitation transfer.

Once we have measured the $5F$ and $5\,^1P$ cross sections at various pressures, we apply Eq. (16) and extract the collisional transfer cross section. We use our experimental values for the $5F\rightarrow 3D$ and $5\,^1P\rightarrow 2\,^1S$ cross sections (as functions of pressure), together with theoretical calculations for the A coefficients [21], as inputs to our model and then calculate the least-squares fit of Eq. (16) to extract the fitting parameters. This process is repeated at each value of the incident electron energy for which data were acquired. The least-squares value of the parameter $\beta_{5\,^1P\rightarrow 5F}$ remained

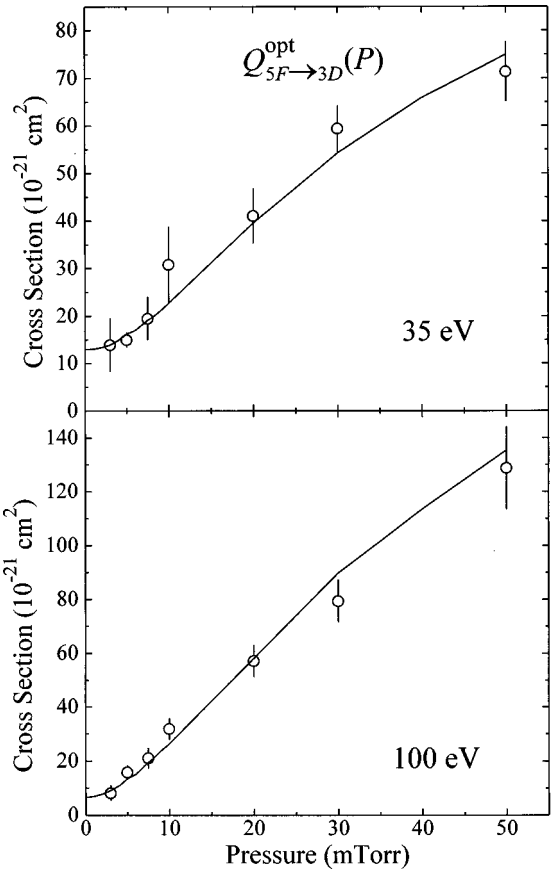

FIG. 6. Optical cross sections for the $5F\rightarrow 3D$ transition versus pressure at 35 and 100 eV. The data have been fit using Eq. (16). The solid curve is calculated from Eq. (16) using the measured $Q^{opt}_{5\,^1P\rightarrow 2\,^1S}(P)$ cross sections and curve-fit parameters for the transfer rate.

quite consistent at all incident electron energies and is equal to $(0.283\pm 0.016)\times 10^6$ mTorr^{-1} s^{-1}, which corresponds to a collisional cross section of $(4.94\pm 1.09)\times 10^{-14}$ cm^2. Figure 6 shows the agreement of the measured $5F\rightarrow 3D$ optical cross sections at pressures from 3 to 50 mTorr at two different electron energies with the calculated values based on Eq. (16) and the curve fit parameters. Since we have measured the $5\,^1P\rightarrow 2\,^1S$ cross sections at pressures as low as 0.08 mTorr and since the $5\,^1P\rightarrow 2\,^1S$ cross section appears to remain constant below 0.08 mTorr at a given electron energy (Fig. 2), we have extended the calculated curve in Fig. 6 down to zero pressure. At each energy, the fit was found to be particularly sensitive to the value of $\beta_{5\,^1P\rightarrow 5F}$. The fit was also found to be highly dependent upon the sum

$$Q^{opt}_{5F_2\rightarrow 3\,^3D}+Q^{opt}_{5F_4\rightarrow 3\,^3D}+(A_{5F\rightarrow 3D}/A_{5F})(Q^{dir}_{5F}+Q^{casc}_{5F}); \quad (18)$$

independently varying the values of the four individual cross section parameters had little effect on the quality of the fit. This sum represents the zero-pressure limit of the $5F\rightarrow 3D$ emission cross section, as indicated in Eq. (17). When we compare the $5F\rightarrow 3D$ cross sections at zero pressure with those at 3 mTorr, we find that even at this low pressure, an appreciable portion of the observed $5F\rightarrow 3D$ signal is due to $5\,^1P\rightarrow 5F$ transfer: 20% at 100 eV and 50% at 200 eV.

TABLE I. Apparent cross sections (at the zero-pressure limit) for the $5\,^1S$, $5\,^1D$, and $5F$ levels versus incident electron energy. Cross sections are expressed in units of 10^{-21} cm^2.

Energy (eV)	$5\,^1S$	$5\,^1D$	$5F$
28	81±10	69±8	26±5
35	92±11	89±11	23±5
40	87±10	90±11	21±4
50	81±10	85±10	18±5
75	67±8	65±8	16±5
100	59±7	51±6	11±3
150	50±6	35±4	8.0±2.4
200	42±5	24±3	6.1±2.2

C. Apparent excitation cross sections for the *nF* levels

From the theoretical transition probabilities of Ref. [21], the branching fraction for the $5F\rightarrow 3D$ decay is found to be 0.64. Upon dividing the zero-pressure $5F\rightarrow 3D$ emission cross sections of Eq. (18) by this branching fraction, we obtain the sum of the apparent excitation cross sections for all the $5F$ levels and the results for electron energies from 28 to 200 eV are shown in Table I. For energy levels conforming to the *LS* coupling, the singlet members generally have much larger cross sections than the triplet ones, except at energies very near the threshold. Thus we include in Table I the $5\,^1S$ and $5\,^1D$ apparent excitation cross sections taken in our laboratory for comparison with the $5F$ results and find the $5\,^1S$ and $5\,^1D$ cross sections considerably larger than those for $5F$, as expected. In Fig. 7 we show the shape of the excitation functions for $5\,^1S$, $5\,^1D$, and $5F$, all normalized to the same maximum height. The $5\,^1S$ and $5\,^1D$ curves show a maximum at about 50 eV in contrast to the 28-eV

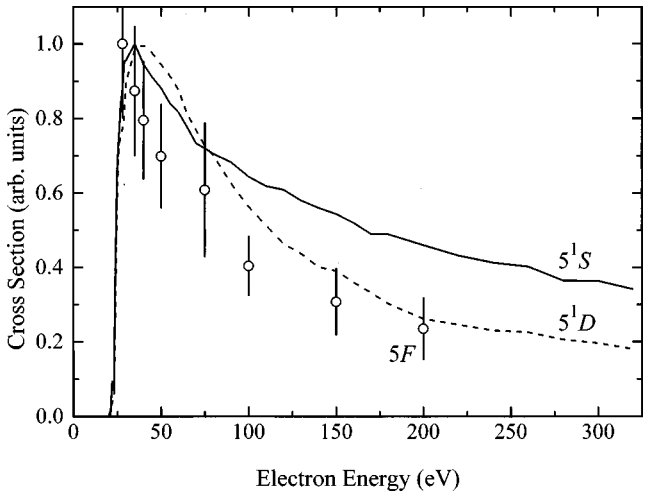

FIG. 7. Apparent excitation functions for the $5\,^1S$ (solid line), $5\,^1D$ (dashed line), and $5F$ (circles) levels. The $5\,^1S$ and $5\,^1D$ excitation cross sections were measured at 0.1 mTorr, where pressure effects are no longer significant. The $5F$ data are the cross sections at the zero-pressure limit. Note the significant difference in shape of the $5F$ excitation function between this plot and the 3-mTorr plot of Fig. 4, indicating the important role of collisional transfer at low (mTorr) pressures. All three curves are normalized to unity at the peak.

TABLE II. Apparent cross sections for the F levels (at the zero-pressure limit) at 50, 100, and 150 eV. Units are 10^{-21} cm^2.

Energy (eV)	$4F$	$5F$	$6F$
50	68±17	18±5	2.9±1.2
100	40±11	11±3	1.8±0.9
150	35±9	8.0±2.4	1.6±0.7

peak exhibited by the $5F$ levels. The $5F$ data appear to decrease about as rapidly with energy as do the $5\,^1D$ cross sections, both consistent with the $1/E$ dependence at high energies. The shape of the $5F$ excitation function shown here differs considerably from the plot of cross section data vs. energy at 3 mTorr in Fig. 4 indicating the influence of collisional transfer even at low pressures of a few mTorr.

From our $4F\rightarrow 3D$ and $6F\rightarrow 3D$ optical emission cross section data taken at different pressures, we also obtain the limiting values for zero pressure, which, together with the appropriate branching fractions calculated from Ref. [21], give the apparent excitation cross sections for the $4F$ and $6F$ manifolds. As explained in Sec. V B, the $4F$ and $6F$ emission signals are more difficult to detect than the $5F$ signal. Thus measurements were made only at 50, 100, and 150 eV. The apparent excitation cross sections at these energies are listed in Table II. Although we have also measured the $7F\rightarrow 3D$ emissions, the uncertainties associated with the very weak signals do not permit a meaningful determination of the zero-pressure cross sections.

Anderson, Hughes, and Norton carried the time-resolution experiments for the $3\,^1D\rightarrow 2\,^1P$ and $3\,^3D\rightarrow 2\,^3P$ emissions to sufficiently low pressures, so that it is possible to extract information about the excitation cross sections (exclusive of the transfer contributions) into the nF levels [9]. These authors reported estimates of excitation cross sections for $4\,^1F$, in units of 10^{-21} cm^2, as 27 ± 7 and 11 ± 5 at 50 and 100 eV, respectively, and 20 ± 5 and 5 ± 2 as the corresponding $4\,^3F$ cross sections. If we add their $4\,^1F$ and $4\,^3F$ cross sections to form the total $4F$ cross section, we find their results to be consistent with ours within the stated uncertainty limits at 50 eV, but below ours at 100 eV.

To obtain the direct excitation cross sections for the nF levels, it is necessary to ascertain the population of these levels due to cascades from the higher D and G levels. The D levels decay predominantly into the P levels with only a small part into the F levels. The branching fractions for the $n\,^1D\rightarrow 4\,^1F(n=5\text{–}7)$, $n\,^1D\rightarrow 5\,^1F(n=6\text{–}8)$, and $n\,^1D\rightarrow 6\,^1F(n=7\text{–}9)$ transitions are no more than 0.005. Thus we can neglect the $D\rightarrow F$ cascades based on any reasonable estimates of the excitation cross sections for the $n\,^1D$ levels. On the other hand, cascades from the G levels are difficult to estimate since we are not aware of any measured cross sections for the G levels. Based on the trend of decreasing cross section with increasing orbital angular momentum, it is reasonable to assume that the cross sections for the G levels are smaller than those of the F levels of the same n. Under this condition, the $G\rightarrow F$ cascades are not expected to constitute a large part of the total population and the apparent excitation cross sections generally can be taken as a first approximation to the direct excitation cross sections.

TABLE III. Our values for the collisional transfer cross sections, determined by measuring emissions from the F levels, are given in the first column. Uncertainties represent systematic and statistical error. The second column lists the values obtained from time-resolved spectroscopic measurements of emissions from the D levels from Ref. [8]. Units are 10^{-14} cm^2.

Level	This work	Ref. [8]
$4F$	1.9±0.5	2.0±0.2
$5F$	4.9±1.1	6.4±0.7
$6F$	11.9±3.5	13±2.6
$7F$	28±11	

D. Cross sections for $n\,^1P\rightarrow nF$ transfer

Section V B indicates that fitting our measured $5F\rightarrow 3D$ and $5\,^1P\rightarrow 2\,^1S$ emission cross sections at various pressures to Eq. (16) determines the value of the excitation transfer parameter $\beta_{5\,^1P\rightarrow 5F}$, which we find to remain constant for all incident energies, as is expected. This parameter is related to the cross section for excitation transfer, $\sigma_{5\,^1P\rightarrow 5F}$, through Eqs. (9) and (12). The same procedure is used to determine the other $n\,^1P\rightarrow nF$ transfer cross sections. Although our data for $n=7$ are limited to a few high-pressure points where the signal is more easily detected, we may still extract the transfer cross section since at high pressures the collisional transfer forms the dominant population process. Our $n\,^1P\rightarrow nF$ transfer cross sections for $n=4\text{–}7$ are given in Table III, which also includes the transfer cross sections reported by Kay and Hughes [8], based on their time-resolution measurements of the $n\,^3D\rightarrow 2\,^3P$ and $n\,^1D\rightarrow 2\,^1P$ emissions. The agreement is seen to be very good. They observed that their transfer cross sections vary as n^4, whereas a log-log plot of our cross sections versus n yields an n^α dependence with $\alpha=4.7\pm 0.7$ (Fig. 8).

The rapid increase of the transfer cross section with n indicates a stronger pressure dependence of the apparent excitation cross section for a higher nF level. For instance, from the zero-pressure limit to 10 mTorr, the apparent excitation cross section at 50 eV increases by a factor of 1.2 for $4F$, 2.7 for $5F$, and 7.9 for $6F$. At 100 eV the correspond-

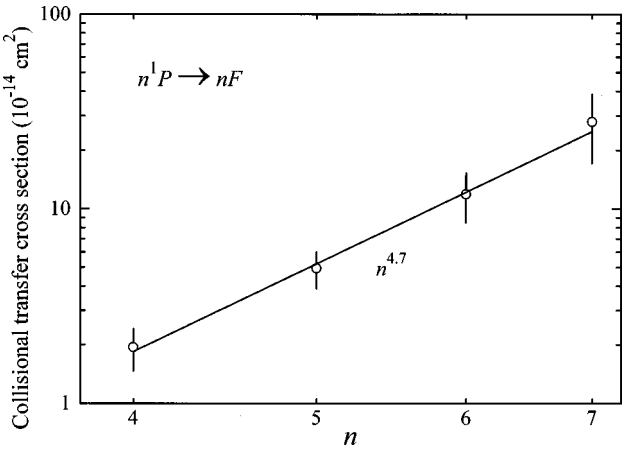

FIG. 8. Collisional transfer cross section for $n\,^1P\rightarrow nF$ versus the quantum number n. A least-squares fit to the data shows that the cross section varies as n^α, where $\alpha=4.7\pm 0.7$.

ing numbers are 1.8 for $4F$, 5.0 for $5F$, and 16 for $6F$. The effect of the $n\,^1P \rightarrow nF$ transfer is most prominent at 100 eV, which corresponds to the peak of the $n\,^1P$ excitation function.

E. Discussion of the transfer model

Finally, some comments should be made concerning the singlet-triplet mixing and its relation to the $n\,^1P \rightarrow nF$ transfer. In Eq. (6) we allow only mixing between singlet and triplet eigenfunctions of the same J based on the fact that J is rigorously a good quantum number for an isolated atom. This led us to the model that allows for transfer from $n\,^1P$ to the two mixed nF_3 levels, but not to the two unmixed $n\,^3F_2$ and $n\,^3F_4$ levels. Kay and Hughes raised the question as to whether the collisional transfer should be so selective [8]. Indeed, St. John and Nee have considered two different transfer models [15]. In their first, the $^3F_2$ and $^3F_4$ states are not operative in the $n\,^1P \rightarrow nF$ collisional transfer, whereas the second model assumes a rapid exchange of excitation among the $n\,^3F_2$, $n\,^3F_3$, and $n\,^3F_4$ states so that all the states in the nF manifold receive transfer from $n\,^1P$. The results of Ref. [15] show a distinct preference for the first model. The role of the $n\,^3F_2$ and $n\,^3F_4$ states in the $n\,^1P \rightarrow nF$ transfer is a complicated issue as it depends on the way in which the nearly degenerate $n\,^3F_2$, $n\,^3F_4$, $n\,F_3^a$, and $n\,F_3^b$ states are perturbed by collision with another atom. Nevertheless, even with a more general model in which transfer from $n\,^1P$ to all F levels of the same n is possible, but with different probabilities, one can adopt an effective cross section for the transfer from $n\,^1P$ to the entire nF manifold so that the pressure dependence of the $5F \rightarrow 3D$ emission cross section can still be described by an analysis similar to the one in Sec. III. Determination of the individual cross sections for transfer into each F level would, of course, depend on the specific transfer model, but the extrapolation of the cross sections to zero pressure remains unchanged. Thus the apparent excitation cross sections for the nF levels are not affected by the transfer model adopted in this paper.

VI. CONCLUSIONS

It has long been known that in electron-impact excitation of helium, the population of the nF levels are strongly influenced by transfer from the $n\,^1P$ levels of the same n through collisions with a ground-state He atom. Direct measurements of the He(nF) atom number density, however, were difficult because emissions from the lower F levels are in the infrared outside the detection range of photomultiplier tubes traditionally used in cross-section measurements. By using the technique of Fourier-transform spectroscopy, we have measured the electron-impact optical cross sections for emission from the nF levels ($n=4-6$) over the target gas pressure range 3–30 mTorr at incident electron energies from threshold to 200 eV. The variations of the emission cross sections with respect to pressure and incident electron energy are in complete accordance with the $n\,^1P \rightarrow nF$ collisional transfer mechanism. Extrapolation of the emission cross-section data to the limit of zero pressure enables us to determine the electron-impact excitation cross sections of the nF, which have not been measured directly before, but only inferred from the time-resolved $n\,^1D \rightarrow 2\,^1P$ and $n\,^3D \rightarrow 2\,^3P$ emission data. Excitation from the ground state to the nF levels involves a large change of the orbital angular momentum. Furthermore, the nF levels are very close to levels of the same n but higher angular momentum and interactions of these nearly degenerate levels induced by the colliding electrons may play an important role. A comprehensive study of the excitation into the nF levels and a comparison with excitation into the levels of lower angular momentum may yet reveal more interesting features of electron excitation processes.

ACKNOWLEDGMENT

This work was supported by the United States Air Force Office of Scientific Research.

[1] J. D. Jobe and R. M. St. John, Phys. Rev. A **5**, 295 (1972).
[2] R. M. St. John and R. G. Fowler, Phys. Rev. **122**, 1813 (1961).
[3] R. L. Abrams and G. J. Wolga, Phys. Rev. Lett. **19**, 1411 (1967).
[4] J. F. Su and J. L. Nicol, J. Phys. B **29**, 4093 (1996).
[5] C. C. Lin and R. G. Fowler, Ann. Phys. (N.Y.) **15**, 461 (1961).
[6] C. C. Lin and R. M. St. John, Phys. Rev. **128**, 1749 (1962).
[7] W. R. Pendleton, Jr. and R. H. Hughes, Phys. Rev. **138**, A683 (1965).
[8] K. B. Kay and R. H. Hughes, Phys. Rev. **154**, 61 (1967).
[9] R. J. Anderson, R. H. Hughes, and T. G. Norton, Phys. Rev. **181**, 198 (1969).
[10] R. B. Kay and C. G. Simpson, J. Phys. B **21**, 625 (1988).
[11] J. E. Chilton, J. B. Boffard, R. S. Schappe, and C. C. Lin, Phys. Rev. A **57**, 267 (1998).
[12] C. A. DeJoseph, Jr. and J. D. Clark, J. Phys. B **23**, 1879 (1990).
[13] J. H. Lees, Proc. R. Soc. London, Ser. A **137**, 173 (1932).
[14] J. H. Lees and H. W. Skinner, Proc. R. Soc. London, Ser. A **137**, 186 (1932).
[15] R. M. St. John and T.-W. Nee, J. Opt. Soc. Am. **55**, 426 (1965).
[16] R. M. Parish and R. W. Mires, Phys. Rev. A **4**, 2145 (1971).
[17] W. H. Wing and W. E. Lamb, Jr., Phys. Rev. Lett. **28**, 265 (1972).
[18] A. R. Filippelli, C. C. Lin, L. W. Anderson, and J. W. McConkey, Adv. At., Mol., Opt. Phys. **33**, 1 (1994).
[19] A. H. Gabriel and D. W. O. Heddle, Proc. R. Soc. London, Ser. A **258**, 124 (1960).
[20] A. R. Filippelli, S. Chung, and C. C. Lin, Phys. Rev. A **29**, 1709 (1984).
[21] C. E. Theodosiou, At. Data Nucl. Data Tables **36**, 98 (1987).